Research Square

Preprints are preliminary reports that have not undergone peer review.
They should not be considered conclusive, used to inform clinical practice,
or referenced by the media as validated information.

Quantifying the High Tang Aesthetic through Geometric and Computational Analysis of Buddhist Sculpture

Luxingyu Liu
Sichuan University
Qiyuan Zhou
Sichuan University
Liang Zhang
Sichuan University
Lingyang Shu
Guangyuan Grottoes Research Institute
Yao Song
yaosong@hkbu.edu.hk

Hong Kong Baptist University

Article

Keywords:

Posted Date: April 2nd, 2026

DOI: https://doi.org/10.21203/rs.3.rs-8827906/v1

License: This work is licensed under a Creative Commons Attribution 4.0 International License.
Read Full License

Additional Declarations: No competing interests reported.

Title:

Quantifying the High Tang Aesthetic through Geometric and Computational Analysis of Buddhist Sculpture

Names and afflictions:

Luxingyu Liu[1#]，Qiyuan Zhou[2#]，Liang Zhang[1#]，Lingyang Shu[3] and Yao Song [2,4,*]

[1] School of Archaeology and Museology, Sichuan University, Chengdu, China.;

[2] Digital Convergence Laboratory of Chinese Cultural Inheritance and Global Communication, Sichuan University, Chengdu, China;

[3] Guangyuan Grottoes Research Institute, Guangyuan, China.

[4] Academy of Chinese, History, Religion and Philosophy, Hong Kong Baptist University

# These authors are co-first authors of the article

* Correspondence: yao.song@connect.polyu.hk

Quantifying the High Tang Aesthetic through Geometric and Computational Analysis of Buddhist Sculpture

Abstract:

Chronological assessment of rock-cut cave heritage often relies on qualitative typological analysis, which remains subjective and lacks metric standardization. This study proposes a quantitative interdisciplinary framework for dating Buddhist sculpture by integrating high-precision 3D laser scanning with Explainable Artificial Intelligence (XAI). Focusing on Tang Dynasty statues from Guangyuan (7th–8th century CE), we analyzed fourteen carefully selected sculptures using a small-sample, high-dimensional strategy. Standardized orthographic projections derived from high-fidelity 3D models enabled extraction of sixteen geometric features. Results reveal a measurable morphological transition: Phase III statues exhibit significant mid-face vertical elongation and reduced workshop standardization, while Phase IV works display a “square-round” morphology driven by vertical facial compression, reflecting High Tang humanistic aesthetics. Machine-learning models, particularly Support Vector Machines and Logistic Regression, achieved 92% chronological classification accuracy. SHAP analysis identifies eye height and eye-to-nose distance as primary determinants of stylistic change, demonstrating a scalable pipeline for computational heritage dating.

1. Introduction

The establishment of precise chronological sequences for rock-cut cave temples constitutes a foundational challenge in Buddhist archaeology and art history. Chronology serves as the necessary framework for reconstructing the dissemination of religious thought[1], regional cultural integration[2], and the evolution of aesthetic paradigms across ancient societies[3]. Traditionally, dating methods have relied on inscriptions, archaeological stratigraphy, and typological analysis[4]. While typology—classifying artifacts based on carving techniques and stylistic traits—remains the dominant method, it faces a critical epistemological bottleneck: the reliance on 'standard sculptures' with explicit dates. In the absence of such benchmarks, dating often devolves into subjective interpretation, where qualitative descriptors such as 'solemn,' 'subtle,' or 'elongated' lack measurable standards. This linguistic ambiguity leads to divergent assessments among scholars for identical artifacts, as perceptual adjectives fail to capture the sub-millimeter geometric shifts that define stylistic evolution[5,6]. Consequently, there is an urgent need to transform these perceptual descriptions into computable metrics, establishing a standardized framework that transcends individual intuition[7,8].

The grottoes of Guangyuan, located in northern Sichuan, exemplify this chronological complexity. As a strategic transportation hub connecting the Central Plains with the Bashu region, Guangyuan served as the primary conduit for the transmission of Buddhist art into Sichuan from the Northern Wei to the Tang Dynasty[9]. Consequently, the region’s sculptures from the 7th to 8th centuries CE (Early to High Tang) capture a

critical “transitional period” in Buddhist art—a shift from the stylistic legacy of the Sui dynasty to the flourishing maturity of the Tang[10]. However, due to the overlapping features of this transition and the natural weathering of stone surfaces, the periodization of these statues remains contentious. The dating of Cave 28 at Huangze Temple offers a salient example of these limitations: academic debate has long oscillated between attributing the cave to the Sui Dynasty[11] or the Early Tang period[12,13]. While recent research utilizing inscriptions has clarified a production date of 602 AD (Sui Dynasty), the stylistic ambiguity that fueled the initial controversy underscores the inability of intuitive stylistic judgment to resolve subtle morphological shifts in the absence of textual evidence[14,15].

The "digital turn" in archaeology offers new pathways to resolve such ambiguities. Recent studies have successfully employed digital modeling and image measurement to analyze facial configurations in Buddhist statuary, from the Sanchi Stupa in India to Japanese sculpture[16-20]. However, existing computational approaches often rely on two-dimensional imagery, which introduces an epistemological bottleneck: perspective distortion. As demonstrated in Fig. 1, 2D photographic analysis is highly susceptible to variations in lighting and shooting angle, where depth-dependent features—such as the curvature of the mouth or the protrusion of the nose—are flattened or skewed. This renders the precise measurement of angular differences impossible and leaves conclusions vulnerable to the subjective positioning of the photographer.

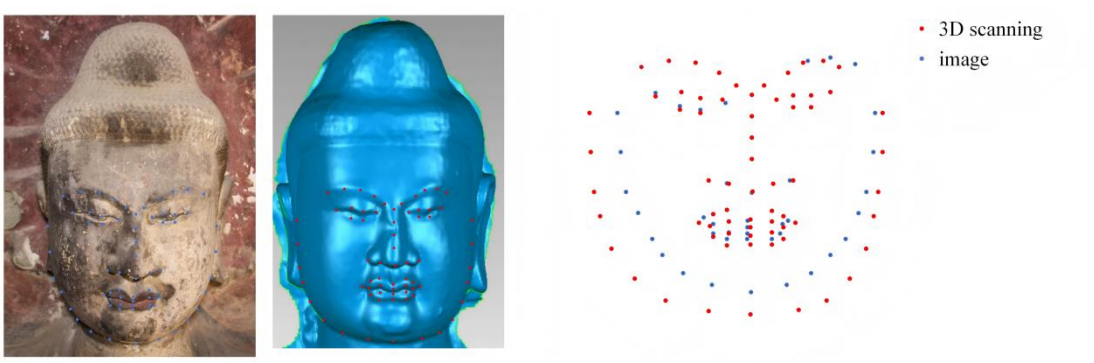


Fig. 1 Comparison between Image Facial Landmark Recognition and 3D Scanning Facial Landmark Recognition

To resolve the fundamental limitations of perspective distortion, this study introduces a metric-faithful workflow that integrates high-precision 3D laser scanning with standardized orthographic projection. Unlike traditional photography, orthographic projection eliminates radial distortion, ensuring that the geometric data fed into our algorithms represents volumetric truth rather than optical illusion[21]. By synthesizing this geometric precision with traditional proportional standards from the Sculpture Measurement Sutra[22] and Explainable Artificial Intelligence (XAI)[23,24], we establish a quantitative, interdisciplinary framework for chronological assessment.

Adopting a “Small-Sample, High-Dimensional” analytical strategy[25], we eschewed the training of universal classifiers on large, noisy datasets in favor of constructing high-fidelity 3D models of 14 rigorously selected, well-preserved statues from the Guangyuan region. Through the transformation of these scans into standardized orthographic projections, we extracted 16 quantifiable geometric features (A–P) and two global indices (SDFP and FSA). This approach transcends subjective stylistic assessment by deconstructing the evolution of the ‘High Tang’ aesthetic into

measurable geometric signals. Consequently, the primary contribution of this work extends beyond the dating of specific statues to the validation of a scalable, metric-faithful pipeline capable of resolving regional controversies in heritage chronology.

2. Methods

2.1 Dataset Construction: Exclusion Protocols for High-Fidelity Geometry

The study focuses on the Tang Dynasty cave temples of Guangyuan, Sichuan—a region that served as a critical node in the transmission of Buddhist art from the Northern Wei to the Tang periods. While the region contains over 3,000 extant statues across sites such as Huangze Temple and Thousand Buddha Cliff, the majority of *in situ* sculptures suffer from severe weathering, exfoliation, or historical damage that compromises the sub-millimeter accuracy required for geometric analysis.

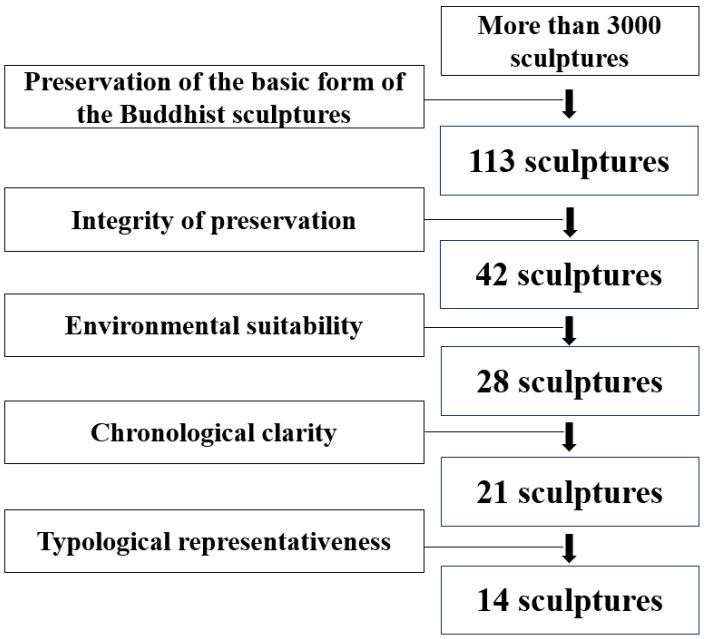


Fig. 2 Screening criteria for selecting Buddha statues

A pervasive challenge in the chronological assessment of ancient cave temples is data scarcity—specifically, the lack of well-preserved samples suitable for high-precision metric analysis. To address this, we employed a 'Small-Sample, High-Dimensional' analytical strategy. Rather than training a universal classifier on a large, noisy dataset containing weathered or restored artifacts, we prioritized data fidelity through a rigorous exclusion protocol. We established a four-stage screening process to identify 'high-fidelity' anchors (N=14) from a population of over 3,000 statues. This approach serves as a reproducible protocol for heritage science, demonstrating that a small, curated dataset of high-dimensional geometric features yields more robust chronological markers than large-scale, low-quality data scraping (Fig. 2): (1) Preservation Integrity: At the initial stage, approximately 113 sculptures were identified as retaining basic morphological features. We further required that the Buddhist heads exhibit no severe loss to critical facial regions (nose, mouth) and no modern restoration interventions, such as repainting or remodeling, that could obscure original carving details. This assessment reduced the pool to 42 sculptures; (2) Environmental Suitability: Among the well-preserved candidates, samples located in niches too deep or narrow for scanner placement, or in environments with excessive humidity or dust that could compromise laser accuracy, were excluded. After on-site evaluation, 28 sculptures were retained; (3) Chronological Clarity: To serve as ground truth for the chronological model, samples required verifiable dating information derived from inscriptions, votive steles, or secure archaeological stratigraphy. This step yielded 21 samples with clear temporal attribution; 4) Typological

Representativeness: Finally, the remaining samples were evaluated for their representativeness of the stylistic features characteristic of the two major historical phases (Phase III and Phase IV).

Ultimately, 14 Buddhist heads were selected as the final dataset (see Table 1). While this sample size (N=14) is small, it represents the exhaustive set of "high-fidelity" artifacts available for reliable 3D reconstruction in this region, ensuring that extracted geometric features reflect original sculptural intent rather than weathering artifacts.

Table 1. Information of collected Buddha statues

No.	Buddha Statues	Staging
1	H38 Main statue on the left wall	Phase III: mid-seventh century (Early Gaozong period)
2	H38 Main statue on the main wall	
3	H38 Main statue on the right wall	
4	H45 Left wall main statue	
5	H45 Main statue on the main wall	
6	Q805 main statue	Phase IV: from the end of the seventh century to the early eighth century (from the Wu Zhou Dynasty to the tenth year of the Kaiyuan Period)
7	Q806-7 Main statue	
8	Q806-34 Main statue	
9	Q806 Left side main statue	
10	Q806 right main statue	
11	Q400 main statue on the right wall	
12	Q400 left wall main statue	

13	Q486 Main statue	
		Not yet determined
14	Q452 Main statue	

Note: H stands for Huangze Temple, Q stands for Thousand Buddha Cliff, and the numbers represent the specific cave numbers. Measurements of the grottoes and statues, as well as descriptions of the niches, follow the records presented in The Comprehensive Record of Guangyuan Grottoes: Huangze Temple Volum[26] and The Comprehensive Record of Guangyuan Grottoes: Thousand Buddha Cliff Volumes I–II[27].

2.2 The Geometric Pipeline: From 3D Laser Scanning to Orthographic Projection

Data acquisition was performed using a high-precision handheld 3D laser scanner (Revopoint[28]), capturing the volumetric morphology of each statue. The raw point cloud data underwent denoising and hole-filling preprocessing to generate watertight mesh models.

A critical innovation in this workflow is the transformation of 3D data into 2D analytical inputs. Unlike traditional photography, which utilizes perspective projection—thereby introducing radial distortion and depth-dependent scaling errors—this study employed orthographic projection via the Open3D visualization engine. This rendering technique eliminates perspective distortion, ensuring that the projected geometry preserves true parallel relationships and relative scale ratios regardless of depth. The resulting standardized frontal images thus serve as metric-faithful maps of the 3D surface, effectively translating volumetric truth into a format compatible with 2D computer vision algorithms without the geometric distortion inherent in standard optical imaging.

2.3 Feature Engineering: Defining the Computational Canon

Buddhist sculptural practice has long been guided by strict canonical standards[29]. Traditional Buddhist teachings describe thirty-two major marks and eighty minor characteristics[30], encompassing all aspects from facial features to the body and even the soles of the feet. As the foremost element of a Buddhist statue, the head serves as the concentrated representation of sculptural style and facial features, reflecting comprehensive norms applied to both global and local aspects of the image. In recent technical art history research, systematic analysis of technical characteristics has been shown to enable the transformation of subjective visual judgments into objective and verifiable parameters, thereby providing a reproducible framework for morphological comparison[31]. Building on this methodological perspective, to quantify the sculptural morphology, we extracted 68 facial landmarks from the orthographic projections using the Dlib facial recognition library[32], validated against manual expert annotation[19]. These landmarks, widely distributed across the facial contour and key features (eyes, eyebrows, nose, mouth), possessing clear anatomical and morphological significance and being widely applied in fields such as facial recognition and expression analysis[33,34] serve as the basis for calculating 16 local geometric features (A–P) and two global indices (see Table 2).

Table 2 Facial geometric indicators of Buddha

Facial geometric features	Code	Feature Formula	Standard Formula	Legend

Eye height	A	$d_A = \lvert \frac{d_{41_y} - d_{37_y} + d_{40_y} - d_{38_y} + d_{47_y} - d_{43_y} + d_{46_y} - d_{44_y}}{4} \rvert$	=A	
Eyebrow to upper eyelid	B	$d_B = \lvert \frac{d_{37_y} - d_{17_y} + d_{38_y} - d_{21_y} + d_{43_y} - d_{22_y} + d_{44_y} - d_{26_y}}{4} \rvert$	=A	
Eye to nose bottom	C	$d_C = \lvert \frac{2\left(d_{31_y} + d_{35_y}\right) - \left(d_{40_y} + d_{41_y} + d_{46_y} + d_{47_y}\right)}{4} \rvert$	=2A	
Nose bottom to chin	D	$d_D = \lvert \frac{\left(d_{6_y} + d_{10_y}\right) - \left(d_{31_y} + d_{35_y}\right)}{2} \rvert$	=4.5A	
Right cheek width	E	$d_E = \lvert d_{16_x} - d_{8_x} \rvert$	=6A	
Left cheek width	F	$d_F = \lvert d_{8_x} - d_{0_x} \rvert$	=6A	
Right chin width	G	$d_G = \lvert d_{10_x} - d_{8_x} \rvert$	=2A	
Left chin width	H	$d_H = \lvert d_{8_x} - d_{6_x} \rvert$	=2A	
Left eyebrow width	I	$d_I = \lvert d_{21_x} - d_{17_x} \rvert$		

Right eyebrow width	J	$d_J = \lvert d_{26_x} - d_{22_x} \rvert$	
Left eye width	K	$d_K = \lvert d_{39_x} - d_{36_x} \rvert$	
Right eye width	L	$d_L = \lvert d_{45_x} - d_{42_x} \rvert$	
Left mouth width	M	$d_M = \lvert d_{51_x} - d_{48_x} \rvert$	
Right mouth width	N	$d_N = \lvert d_{54_x} - d_{51_x} \rvert$	
Left nose width	O	$d_O = \lvert d_{33_x} - d_{31_x} \rvert$	
Right nose width	P	$d_P = \lvert d_{35_x} - d_{33_x} \rvert$	
Smile degree	Q	$d_Q = \arctan\lvert \frac{d_{48_y} - d_{57_y}}{d_{48_x} - d_{57_x}} \rvert$	
Facial width-to-height ratio	R	$d_R = \lvert \frac{d_{0_x} - d_{16_x}}{d_{0_y} - d_{3_y}} \rvert$	

2.3.1 Local Geometric Features and Normalization

To ensure consistency across statues of varying physical sizes, all measurements were normalized by the Face Width. Face Width was selected as a conservative and stable reference dimension that captures the overall facial scale while remaining minimally affected by local stylistic variation, facial expression, or minor geometric distortion introduced during orthographic projection. In the context of heritage science, such a global normalization reference facilitates reproducible and non-invasive comparison across objects of different sizes without introducing circular dependence on the local features under investigation. Face Width is defined as the horizontal span of the minimal bounding rectangle encompassing all 68 facial landmarks:

$$Face\ Width = max(x_{0\ldots67}) - min(x_{0\ldots67})$$

Based on the extracted facial landmarks, we defined 16 geometric features (A–P) and derived ratios. All geometric features were computed from landmark coordinates. Distance-based features were normalized by Face Width to ensure scale invariance, according to

$$i = \frac{d_i}{Face\ Width}$$

where i denotes the original geometric distance. Ratio-based features were calculated as proportions between relevant facial dimensions and are therefore inherently scale-independent, without further normalization.

2.3.2 Global Standardization Metrics

To evaluate the adherence of statues to iconometric canons, we defined the Standard Deviation of Facial Proportions (SDFP). This index measures the aggregate deviation

of a statue's features from the idealized ratios recorded in the Sculptural Measurement Sutra. Unlike individual geometric features, the SDFP utilizes the "A" unit (Canonical Eye Height) as a theoretical benchmark.The SDFP is calculated as:

$$SDFP = \sum_{i \in \{A \ldots H\}} \left| \frac{Feature_i}{Standard_i} - 1 \right|$$

Where a value closer to 0 indicates higher standardization and strict adherence to the canonical workshop templates.

2.3.3 Symmetry Analysis

To quantify the "solemnity" and technical precision of the carving, we defined the Facial Symmetry Aesthetics (FSA) index. This metric calculates the cumulative asymmetry between bilateral feature pairs (e.g., Left Eye Width K vs. Right Eye Width L):

$$FSA = \sum_{(x,y) \in Pairs} \left| \frac{X}{Y} - 1 \right|$$

Where a lower FSA value signifies higher bilateral symmetry, reflecting the High Tang pursuit of "perfect harmony".

2.4 Analytic Strategy: Robust Machine Learning for Small-Sample Data

Given the "Small-Sample, High-Dimensional" nature of the dataset (N = 14), conventional deep learning approaches are susceptible to overfitting. Therefore, this study adopted an analytical strategy focusing on classifiers with strong inductive biases suitable for small datasets (see Fig. 3)[35,36].

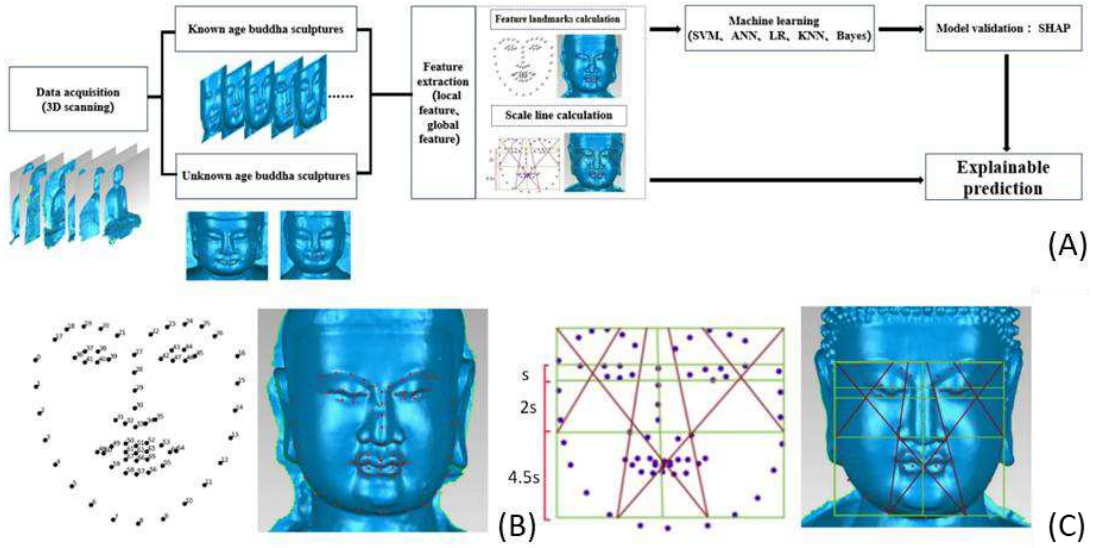


Fig. 3 The computational framework for chronological assessment and geometric feature engineering. (A) The methodological pipeline integrating high-precision 3D scanning, standardized orthographic projection, and Explainable Artificial Intelligence (XAI) to resolve chronological ambiguity. The workflow progresses from data acquisition to feature extraction, followed by multi-model machine learning classification (SVM, ANN, LR, KNN, Bayes) and SHAP-based model validation. (B) Extraction of 68 fiducial facial landmarks from the standardized orthographic projection, mapping the contours of the eyes, eyebrows, nose, mouth, and jawline. (C) Geometric feature construction based on traditional iconometric canons (Sculptural Measurement Sutra). The grid illustrates the derivation of proportional features (e.g., C, D, R) relative to the basic measurement unit S, defined as one Eye Height.

We employed and compared five algorithms: Support Vector Machines (SVM), Logistic Regression (LR), K-Nearest Neighbors (KNN), Naïve Bayes, and Artificial Neural Networks (ANN[37]). Priority was placed on SVM and Logistic Regression due to their margin-maximization properties and interpretability. To rigorously validate model performance, Leave-One-Out Cross-Validation (LOOCV[38]) was utilized[39]. This method provides nearly unbiased estimates of prediction error for small datasets, ensuring that the identified chronological determinants are robust stylistic markers. Finally, SHAP(SHapley Additive exPlanations)[40] was applied to interpret the decision logic of the models, identifying the specific geometric features driving the

chronological classification[41].

3. Results

3.1 Geometric Divergence: Statistical Evidence of the Stylistic Transition

A comparative analysis of the 14 Buddhist statues reveals a quantifiable morphological rupture between the mid-seventh century (Phase III) and the late-seventh/early-eighth century (Phase IV). As detailed in Table 3, Mann-Whitney U tests identified statistically significant differences ($P < 0.05$) in 7 of the 18 examined geometric features, confirming that the stylistic transition is not merely impressionistic but geometrically structural (see Table 3 and

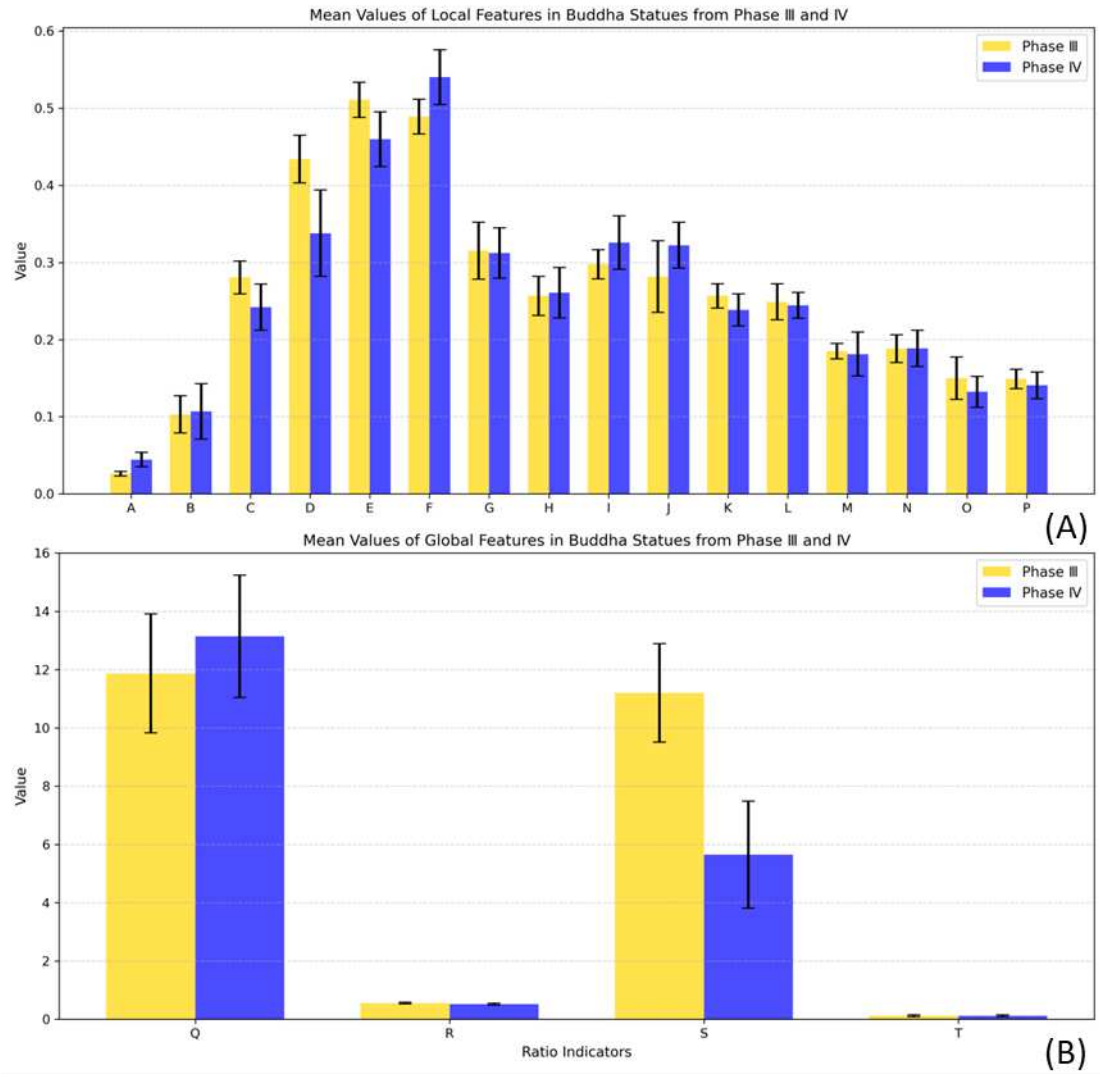


Fig. 4).

Table 3 Descriptive analysis and statistical differences of overall features.

		Phase III (Mean±SD)	Phase IV (Mean±SD)	Mann-WhitneyU		
				U	P	r
Local features	A	0.0263±0.0029	0.0445±0.0093	0	0.0025	0.8204
	B	0.1030±0.0241	0.1069±0.0360	16	0.8763	0.0703
	C	0.2806±0.0214	0.2422±0.0299	31	0.0303	0.6329
	D	0.4341±0.0309	0.3379±0.0559	32	0.0177	0.6798

	E	0.5108±0.0227	0.4597±0.0355	32	0.0177	0.6798
	F	0.4892±0.0227	0.5403±0.0355	3	0.0177	0.6798
	G	0.3154±0.0369	0.3124±0.0327	19	0.8763	0.0703
	H	0.2567±0.0254	0.2610±0.0328	18	1	0.0234
	I	0.2978±0.0189	0.3260±0.0347	8	0.149	0.4454
	J	0.2817±0.0465	0.3224±0.0298	7	0.1061	0.4922
	K	0.2567±0.0157	0.2384±0.0208	27	0.149	0.4454
	L	0.2490±0.0234	0.2445±0.0169	21	0.6389	0.1641
	M	0.1850±0.0099	0.1812±0.0285	17	1	0.0234
	N	0.1882±0.0180	0.1886±0.0235	16	0.8763	0.0703
	O	0.1500±0.0276	0.1324±0.0201	25	0.2677	0.3516
	P	0.1490±0.0125	0.1406±0.0173	21	0.6389	0.1641
	Q	11.8683±2.0427	13.1411±2.0984	12	0.4318	0.2578
	R	0.5519±0.0258	0.5222±0.0313	27	0.149	0.4454
Global features	S	11.1979±1.6895	5.6508±1.8374	35	0.0025	0.8204
	T	0.1185±0.0288	0.1159±0.0315	19	0.8763	0.0703

Note: Q represents the smile extent index, R corresponds to the facial width-to-length ratio (fWHR), S denotes the SDFP index, and T indicates the FSA index.

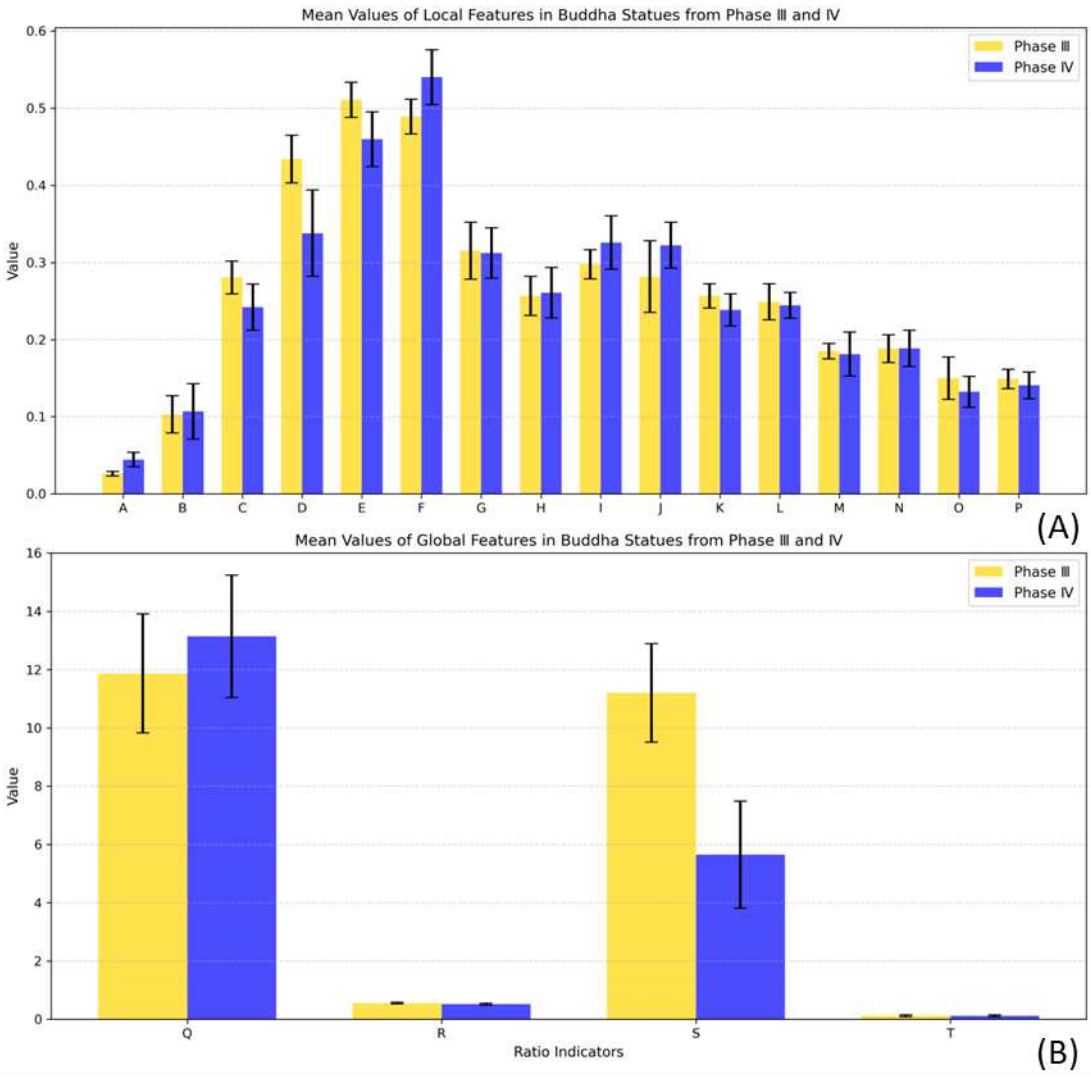


Fig. 4 Statistical divergence of facial geometric features between Phase III (Early Tang) and Phase IV (High Tang) statues. (A) Comparison of Local Features (A–P): Bar charts display Mean ± SD (Standard Deviation). Statistically significant differences ($P < 0.05$) are observed in the vertical expansion of Eye Height (A) and the vertical compression of the mid-face (C) and lower-face (D) in Phase IV. (B) Comparison of Global Features (Q, R, S, T): The dramatic reduction in the Standard Deviation of Facial Proportions (S) in Phase IV indicates a shift toward rigorous workshop standardization. The Smile Degree (Q) shows an increasing trend, correlating with the secularization of the High Tang aesthetic.

3.1.1 Vertical Dimensions and Ocular Expansion

The most pronounced divergence occurred in the vertical dimensions of the face.

While the global Facial Width-to-Height Ratio (R) exhibited only a slight, non-

significant decrease from 0.5519 in Phase III to 0.5222 in Phase IV ($P > 0.05$) , the internal vertical structure underwent significant compression. The vertical distances from the Eye to Nose Bottom (C) and from the Nose Bottom to the Chin (D) showed a marked reduction in Phase IV statues. Specifically, Feature C decreased from a mean of 0.2806 ± 0.0214 in Phase III to 0.2422 ± 0.0299 in Phase IV (P = 0.03), while Feature D dropped significantly from 0.4341 ± 0.0309 to 0.3379 ± 0.0559 (P = 0.01).

Simultaneously, the eye structure underwent a significant vertical expansion. The Eye Height (A) increased from 0.0263 ± 0.0029 in Phase III to 0.0445 ± 0.0093 in Phase IV (P < 0.01). In contrast to this vertical opening, the horizontal width of the eyes remained relatively stable or slightly contracted: Left Eye Width (K) shifted from 0.2567 ± 0.0157 to 0.2384 ± 0.0208, and Right Eye Width (L) from 0.2490 ± 0.0234 to 0.2445 ± 0.0169. The significant increase in standard deviation for Phase IV eye widths reflects a departure from strict uniformity toward greater diversity in sculptural styles.

3.1.2 The "Smile" (Feature Q)

Beyond structural geometry, the analysis of emotional expression via the Smile Degree (Q) reveals a distinct upward trend. The mean smile angle increased from 11.8683 ± 2.0427 in Phase III to 13.1411 ± 2.0984 in Phase IV. Although this increase did not reach statistical significance (P > 0.05) likely due to sample size, the rising mean values provide a quantitative correlate to the stylistic shift described in

traditional art history: a transition from the “solemn and dignified” aesthetic of the Early Tang toward the more “compassionate and approachable” demeanor of the High Tang.

3.2 The "Square-Round" Morphology: Deconstructing the Vertical Compression

While traditional art historical scholarship characterizes the High Tang style as "square-round" (fang yuan), our geometric decomposition refines this definition. The Facial Width-to-Height Ratio (R), a global metric often used to quantify facial robustness, exhibited a slight downward trend from 0.5519 ± 0.0258 in Phase III to 0.5222 ± 0.0313 in Phase IV. Notably, this difference was not statistically significant ($P > 0.05$), indicating that the external "bounding box" or the absolute silhouette of the head did not undergo a radical transformation.

However, the perception of a "Square-Round" or "fuller" face in Phase IV is strongly driven by the statistically significant vertical compression of internal features. As detailed in Section 3.1, the mid-face length (C) and lower-face height (D) decreased significantly ($P < 0.05$). This internal compaction lowers the visual center of gravity, creating a sense of density and volume in the lower face without necessitating a widening of the cranial outline. Thus, the "High Tang" aesthetic is geometrically defined not by a change in the frame (R), but by the densification of the content (C and D) within that frame, creating the visual illusion of roundness through vertical compactness.

Furthermore, a decomposition of the ratio components isolates the mechanism of this shift. While horizontal cheek widths exhibited complex, asymmetrical variance—Right Facial Width (E) decreased (0.5108 → 0.4597) while Left Facial Width (F) increased (0.4892 → 0.5403)—these fluctuations were not the decisive drivers. The "High Tang" aesthetic is therefore geometrically defined not by a change in the frame (R), but by the densification of the content (C and D) within that frame. This vertical compaction alters the internal aspect ratio, creating the visual illusion of roundness and volume through vertical compactness rather than horizontal expansion.

3.3 Global Standardization and the "Tipping Point"

In terms of global standardization (Fig. 5), the Standard Deviation of Facial Proportions (SDFP) displayed the highest statistical separability ($P < 0.01$). The mean SDFP dropped dramatically from 11.1979 ± 1.6895 in Phase III to 5.6508 ± 1.8374 in Phase IV. This indicates a marked improvement in proportional standardization, reflecting the establishment of a rigorous workshop canon during the High Tang period. Similarly, the Facial Symmetry Aesthetics (FSA) values remained low across all samples but improved slightly in Phase IV (0.1185 vs 0.1159), indicating a persistent and refining pursuit of bilateral balance.

A longitudinal analysis of the individual statues reveals a specific "tipping point" in the evolution of these global features. As illustrated in the trajectory of the 12 dated statues (Fig. 5), the trends for both SDFP and FSA shift noticeably between Statue 5 and Statue 8. The earlier statues (Phase III) exhibit higher variability and SDFP

values, consistent with a transitional period of stylistic adaptation. From Statue 6 onwards (Phase IV), the values stabilize near zero, marking the maturation of the High Tang style where standardization and symmetry were integrated into the sculptural practice.

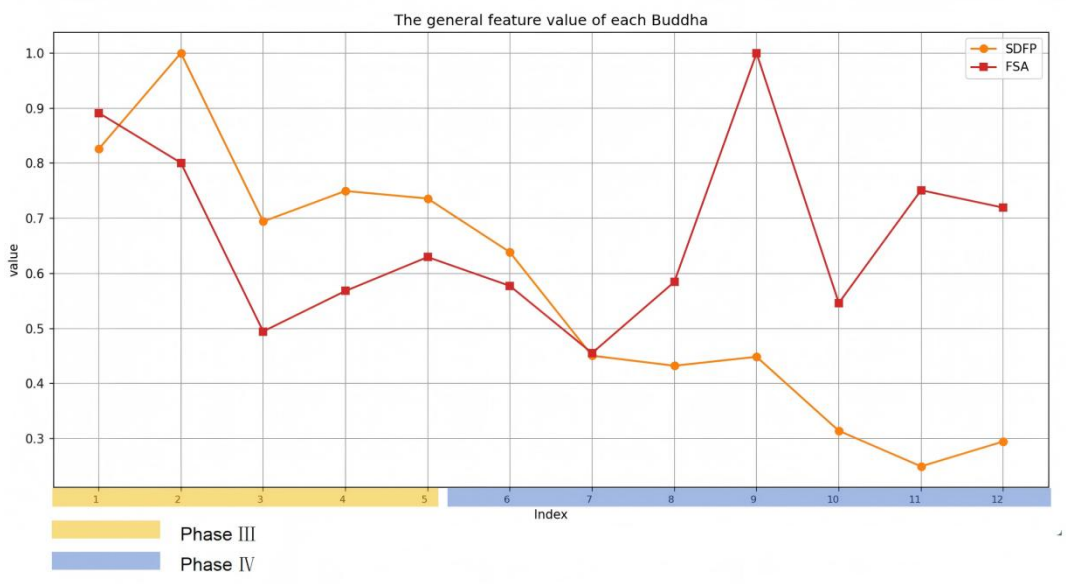


Fig. 5 Mean values of the features across statues

3.4 Predictive Modeling and Feature Attribution

The discriminative power of these geometric features was rigorously validated through supervised machine learning using Leave-One-Out Cross-Validation (LOOCV). Among the five algorithms tested, the linear margin-based models—Support Vector Machine (SVM) and Logistic Regression (LR)—demonstrated the highest robustness, both achieving a classification accuracy of 92%. The K-Nearest Neighbors (KNN) model followed with 83% accuracy, while the nonlinear Artificial Neural Network (ANN) and probabilistic Naïve Bayes classifiers exhibited comparatively lower performance at 75%. When applied to the statues with

ambiguous dating (No. 13 and No. 14), the models demonstrated varying degrees of consensus. Statue 13 was unanimously classified as Phase IV by all five algorithms, providing strong computational support for its attribution to the High Tang period. Statue 14, however, elicited a slight divergence: the top-performing models (SVM, LR, and KNN) classified it as Phase III, whereas the lower-accuracy models (ANN and Bayes) assigned it to Phase IV. Given the superior cross-validation stability of the linear classifiers, Statue 14 is attributed to Phase III (Early Tang) with high confidence. To move beyond "black box" classification, SHAP (SHapley Additive exPlanations) analysis identified Eye Height (A) and Eye-to-Nose Distance (C) as the primary determinants of the model's decision boundary (see Fig. 6). Specifically, low values for Eye Height (A) and high values for vertical mid-face length (C) drive the model to classify a sample as Phase III. This computational attribution aligns perfectly with the statistical findings, identifying the "closed eye, long mid-face" configuration as the mathematical fingerprint of the Early Tang/Sui legacy.

3.5 Robustness Analysis of Normalization Metrics

To assess the robustness of the normalization strategy, key analyses were repeated using alternative global facial references, including facial height and the diagonal length of the minimal bounding rectangle encompassing all facial landmarks. Comparable patterns of morphological differences were observed across normalization schemes, indicating that the reported results are not driven by the specific choice of Face Width.



Fig. 6 Explainable AI (XAI) analysis of the chronological decision boundaries. (A) SHAP global importance plots for Support Vector Machine (SVM), Logistic Regression (LR), and K-Nearest Neighbors (KNN). The x-axis represents the mean absolute SHAP value, quantifying the overall magnitude of each feature's contribution. (B) SHAP beeswarm plots illustrating the directionality of feature impact. Each dot represents a single statue sample. Interpretation Guide: The color indicates the actual geometric measurement (Red = High Value; Blue = Low Value). The position on the x-axis indicates the impact on the model's decision: dots shifted to the right (positive SHAP value) increase the probability of classifying the statue into the target phase. Example: In the Phase III panel (left column), the feature Eye-to-Nose Distance (C) shows red dots clustered on the right side. This indicates that high values of Feature C (a longer mid-face) increase the probability of Phase III classification, mathematically confirming the "long mid-face" aesthetic of the Early Tang. Conversely, Eye Height (A) shows blue dots on the right, meaning low values (narrower eyes) are predictive of Phase III.

4. Discussion

The geometric data extracted from the Guangyuan statues provides empirical

evidence for a fundamental shift in the visual construction of religious authority during the Tang Dynasty. By 'quantifying the intangible,' this study bridges the gap between metric data and art historical theory, demonstrating that the stylistic transition is not merely impressionistic but a quantifiable restructuring of the theological interface. We argue that the transition is driven by a synergy of three geometric mechanisms—vertical compression, ocular expansion, and the secularization of expression—which collectively mark the migration of the divine image from a transcendent "icon of awe" to an immanent "icon of compassion."

Phase III statues (Early Tang) are geometrically continued the regal style of the Northern Zhou and Sui dynasties. They are defined by significant vertical elongation in the mid-face (C) and lower-face (D) combined with narrower eye openings (A). This "long-oval" morphology which means higer Facial Width-to-Height Ratio (R) creates a visage of distance and authoritativeness. In evolutionary psychology and anthropological aesthetics, a higher FWHR is frequently associated with perceived dominance and aggression[42]. As a projection of the rulers' ideology, Buddhist statues served as instruments for maintaining a rigid social hierarchy[43]. This sense of imposing solemnity heightened the faithful's perception of the Buddha, imbuing the divine image with a regal posture that surveys all living beings from above.Beyond feature R, this theological distance is also quantitatively corroborated by the low Smile Degree (Q) observed in Phase III (11.87˚). These statues display minimal upward lift of the mouth corners, reflecting an "expressionless" or "micro-expression" aesthetic designed to evoke a sense of reverence and worship in the devotees,

suppressing individual emotion in favor of universal authority. The geometric configuration of Phase III—combining a relatively higher FWHR with the "expressionless" closed mouth (Q=11.87˚)—constructs a visage of formidable power. This aligns with the Early Tang political mandate, where Buddhism served as a state-sanctioned instrument of ideological consolidation.

In contrast, Phase IV (High Tang) statues exhibit a "humanistic" reconfiguration. The reduction in the mean FWHR (R) to 0.52 in Phase IV, while statistically subtle, correlates theoretically with the shift toward approachability. Lower width-to-height ratios are often associated with reduced perceptions of threat and increased trustworthiness[44].The statistically significant reduction in vertical facial dimensions ($P < 0.05$) lowers the visual center of gravity, generating the "Square-Round" (fang yuan) aesthetic. While traditional art history attributes this to "fullness," our data proves that this perceived volume is achieved not by widening the face, but by compacting the vertical midline. Theoretically, this vertical compression brings the deity "down to earth," replacing the aristocratic elongation of the Early Tang with a robust, earthy solidity that aligns with the High Tang ideal of grand style[45]. This structural compression is accompanied by a significant increase in Eye Height (A, $P < 0.01$), resulting in fuller, rounder eyes that align with Secularization. Most critically, the geometric data captures the secularization of the smile. The increase in Smile Degree (Q) to 13.14˚ in Phase IV correlates with the visual prominence of the lips in human emotional perception. This interaction between the "benevolent" open eyes and the softened mouth corners reflects the socio-political transformation of the High

Tang, where Buddhism transitioned from an aristocratic religion to a "popular faith"[46],where the visual language of the deity evolved from a code of dominance (High R, Low Q) to a code of compassion (Lower R, High Q), facilitating a direct emotional connection with the lay practitioner[47,48].

Beyond theological expression, the global geometric features serve as computational proxies for the sociological organization of the local artisan workshops. We propose the Standard Deviation of Facial Proportions (SDFP) as a quantitative metric for craftsmanship evolution. The dramatic reduction of SDFP from 11.20 in Phase III to 5.65 in Phase IV indicates a transition from an experimental, heterogeneous production environment to a highly standardized, quasi-industrial workshop system.

In the mid-seventh century (Phase III), the high SDFP reflects a period of "adaptive friction." Many sculptors were monks or artisans recently arrived from the Northern Central Plains. These immigrant craftsmen were likely reconciling northern templates (Zhou-Sui legacies) with local geological conditions and indigenous techniques, resulting in high variability and "transitional" deviations from canonical proportions[49]. By the late seventh century (Phase IV), the low SDFP signals the successful establishment of a rigorous local canon. The artisan community in Guangyuan may have matured, developing the technical capability to achieve precise proportional control while strictly adhering to the Sculptural Measurement Sutra. This evolution mirrors the broader flourishing of the High Tang, where the philosophy of art sought to balance normative precision (canon) with aesthetic refinement (expression).

Furthermore, the integration of high facial symmetry (low FSA values) in Phase IV reflects the specific High Tang philosophical pursuit of "perfect harmony" [50],where bilateral balance was employed to reinforce the visual stability of the "square-round" facial morphology[51]. The computational evidence thus maybe charts the trajectory of the Guangyuan grottoes from a transitional grotto site to a mature regional center of artistic production.

The primary contribution of this work extends beyond the regional chronology of Guangyuan; it validates a scalable, data-driven pipeline for the broader field of digital heritage. We demonstrate that the transformation of 3D laser scanning data into standardized orthographic projections effectively bridges the gap between volumetric fidelity and current computer vision capabilities.

Unlike 2D photography, which is compromised by perspective distortion and lighting variance—rendering measurements of depth (e.g., mouth curvature) unreliable—our orthographic pipeline preserves the metric truth of the artifact. This ensures that features like "Eye Height" are measurements of geometry rather than shadow, providing a stable baseline for analysis.

Consequently, this framework offers a methodological prototype for researchers working in 'data-scarce' environments common to archaeology. By defining facial geometric features as quantitative 'stylistic fingerprints,' we demonstrate that machine learning models—specifically SVM and Logistic Regression—can achieve high accuracy (92%) even with small sample sizes (N=14), provided the input data

preserves true geometric proportions. While the sample size is numerically small, the statistical significance ($P < 0.05$) observed in key features (A, C, D, S) confirms that the signal-to-noise ratio in this high-fidelity dataset is sufficient for robust classification.

This validates a 'quality-over-quantity' approach, offering a reproducible solution for objectively dating unprovenanced museum collections or damaged heritage assets where massive training sets are unavailable. Furthermore, this high-fidelity geometric data lays the groundwork for next-generation applications in Digital Twins and Generative AI, where 'standardized' morphological features could guide the scientifically grounded virtual reconstruction of weathered cultural heritage.

Notably, this paradigm of translating perceptual stylistic judgments into objective, verifiable evidence aligns with pioneering work in art historical technical analysis. Ainsworth discovered the double authorship of The Annunciation attributed to Memling in the Metropolitan Museum of Art via infrared reflectography, converting intuitive observations of Rogier van der Weyden-like preparatory sketches into tangible underdrawing evidence[52]. Similarly, our study leverages 3D scanning, orthographic projection, and Explainable AI to deconstruct the "High Tang aesthetic"—a traditionally subjective concept—into quantifiable geometric metrics. Together, these works underscore the transformative potential of technical tools in resolving ambiguity in cultural heritage research, offering a replicable reference for translating intangible stylistic traits into data-driven evidence across diverse art

historical and archaeological contexts.

While this study successfully establishes a geometric-computational framework for chronological assessment, certain limitations inherent to the "Small-Sample, High-Dimensional" strategy must be acknowledged. First, the dataset was strictly limited to 14 high-fidelity samples to ensure sub-millimeter geometric accuracy. Although Leave-One-Out Cross-Validation (LOOCV) confirmed the robustness of the probabilistic models (92% accuracy), the small sample size precludes the use of data-hungry Deep Learning architectures, such as Convolutional Neural Networks (CNNs), which require massive training sets to generalize effectively. Future research aims to expand this dataset by incorporating samples from comparable grotto sites, potentially employing transfer learning techniques[53] to adapt the current SVM and Logistic Regression models to larger, more diverse populations.

Second, the current analysis is geographically confined to the Guangyuan region, a "transitional node" between the Central Plains and the Bashu region. It remains to be verified whether the specific geometric indicators of the "High Tang" style identified here—such as the vertical compression of the mid-face (Feature C) and the expansion of the eye (Feature A) are universal markers of the Tang dynasty aesthetic or specific regional adaptations. Future work will apply this orthographic pipeline to core metropolitan sites, such as the Longmen and Dunhuang grottoes[54], to construct a pan-regional "geometric map" of stylistic dissemination[55].

Finally, the high-precision geometric data extracted in this study lays the groundwork

for advanced applications in computational restoration. The quantitative "stylistic fingerprints" identified here can serve as parametric constraints for Generative AI and Digital Twin technologies. By inputting the standardized "High Tang" ratios (e.g., low SDFP and specific facial proportions) into generative adversarial networks (GANs), researchers could scientifically guide the virtual reconstruction of damaged or weathered statues[56]. This would transform digital heritage from a passive descriptive tool into an active, scientifically grounded instrument for virtual conservation.

Data availability

The data that support the findings of this study are available from the corresponding author upon reasonable request.

Acknowledgments

The research was supported by a Start-up Grant from HKBU, the Start-Up Research Fund from FASS at HKBU, and the Sichuan University Interdisciplinary Innovation Fund.

Author contributions

L.L., Q.Z., and L.Z. contributed equally to this work. Y.S. conceptualized the study, developed the methodology, and acquired funding. L.L. and L.Z. conducted the archaeological investigation, artifact screening, and historical contextualization. Q.Z. performed the 3D laser scanning, geometric feature extraction, and machine learning/XAI analysis. L.S. provided site access, expert guidance, and archaeological validation at the Guangyuan Grottoes. L.L., Q.Z., and L.Z. drafted the main manuscript. Y.S. supervised the research and critically revised the manuscript. All authors reviewed and approved the final manuscript.

Competing Interests

The authors declare no financial or non-financial competing interests.

References

1. Zhao, H., Lee, J., Ye, X. & Tyner, J. Spatiotemporal analyses of religious establishments in coastal China. *GeoJournal*, 82, 971–986 (2017). https://doi.org/10.1007/s10708-016-9726-y

2. Birch, J., Manning, S. W., Sanft, S. & Conger, M. A. Refined radiocarbon chronologies for northern Iroquoian site sequences: Implications for coalescence, conflict, and the reception of European goods. *American Antiquity*, 86, 61–89 (2020). https://doi.org/10.1017/aaq.2020.73

3. Carden, N., Martínez, G., Mitchell, P. & Orton, J. Spatial and temporal trends in the distribution of engraved eggshell fragments: A comparative view from the Holocene archaeological record of southern Africa and southern South America. *Journal of Anthropological Archaeology*, 73, 101571 (2024). https://doi.org/10.1016/j.jaa.2024.101571

4. Fu, Y. L., & Zhao, S. Q. Methods for dating cliff carvings (moya zaoxiang). *Journal of Popular Archaeology*, 10 (2023) (in Chinese).

5. Ugail, H., Stork, D. G., Edwards, H. & Brooke, C. Deep transfer learning for visual analysis and attribution of paintings by Raphael. *Heritage Science*, 11, 268 (2023). https://doi.org/10.1186/s40494-023-01094-0

6. Wang, S., Liu, S., Jin, M. & Yuan, M. Emotion recognition in Dunhuang Mogao mural figures via PNASNet-CBAM. *npj Heritage Science*, 13, 384 (2025). https://doi.org/10.1038/s40494-025-01961-y

7. Gilboa, A., Karasik, A., Sharon, I. & Smilansky, U. Towards computerized typology and classification of ceramics. Journal of Archaeological Science, 31, 681–694 (2004). https://doi.org/10.1016/j.jas.2003.10.013

8. Wang, J., Qian, W. & Chen, G. Combining quantitative analysis with an elliptic Fourier descriptor: A study of pottery from the Gansu-Zhanqi site based on 3D scanning and computer technology. *Journal of Archaeological Science: Reports*, 36, 102897 (2021). https://doi.org/10.1016/j.jasrep.2021.102897

9. Lei, Y. H., Luo, C. X., & Wang, J. P.*Study on buddhist grottoes and cliff carvings in northern sichuan*. Gansu Education Press (2016) (in Chinese).

10. Yao, C. X. Preliminary study on buddhist grotto statues in bashu area: Focusing on northern sichuan. Zhonghua Book Co. (2011) (in Chinese).

11. Yan, W. R. Qianfo cliff and huangze temple in guangyuan, sichuan. *Jianghan Archaeology*, 3 (1990) (in Chinese).

12. Guangyuan Municipal Institute of Cultural Relics Management, et al. Investigation record of huangze temple grottoes in guangyuan. *Cultural Relics*, 6 (1990) (in Chinese).

13. Wen, Y. C. *Chinese grottoes and their cultural art*. Shanghai People's Fine Arts Publishing House (1993) (in Chinese).

14. Guangyuan Huangze Temple Museum. Textual research on the age of cave no. 28 in huangze temple, guangyuan. *Sichuan Cultural Relics*, 1 (2004) (in Chinese).

15. Wang, J. P. Further research on the age of cave no. 28 in huangze temple, guangyuan: Also on the style and origin of its sculptural art. In Dazu Rock Carvings Research Institute (Ed.), *Proceedings of the 2005 international academic conference on dazu rock carvings, chongqing* (pp. 594–599). Wenwu Press (2007) (in Chinese).

16. Dixit, M., Singh, A., & Gupta, S. Digital documentation and analysis of buddhist sculptures: A case study of sanchi stupa. *Journal of Cultural Heritage*, 32, 145–153 (2018).

17. Ikeuchi, K., Sato, Y., & Miyazaki, D. 3D modeling and analysis of japanese buddhist statues

for preservation and research. *Computer Vision and Image Understanding*, 145, 89–102 (2016).

18. Renoust, B., & Nakamura, M. Machine learning for the analysis of facial proportions in japanese buddhist sculpture. *Journal of Archaeological Science*, 107(10), 50–87 (2019).

19. Yang, Y., Zhang, H., & Li, J. Quantitative analysis of facial features in tibetan thangka buddha statues based on dlib algorithm. *Journal of Digital Imaging*, 33(4), 890–898 (2024).

20. Wei, S., Hou, M., & Yang, S. Semantic segmentation of Buddha facial point clouds through knowledge-guided region growing. npj *Heritage Science*, 14, 109 (2026).

21. Li, T., Jiang, C., Bian, Z., Wang, M., & Niu, X. (2020). A Review of True Orthophoto Rectification Algorithms. *IOP Conference Series: Materials Science and Engineering*, 780(2), 022035. https://doi.org/10.1088/1757-899x/780/2/022035

22. Gacang. *Tibetan buddhist thangka measurement sutra*. Qinghai Nationalities Publishing House (1992) (in Chinese).

23. Jiang, X., Harun, S. N. & Liu, L. Explainable Artificial Intelligence for Ancient Architecture and Lacquer Art. *Buildings*, 13, 1213 (2023).

24. Cho, Y. E., Sim, S., Choi, J. & Ahn, S. Explainable machine learning-based classification of traditional Korean ceramics using XRF chemical composition data. *npj Heritage Science*, 14, 28 (2026). https://doi.org/10.1038/s40494-026-02301-4

25. Todman, L. C., Bush, A. & Hood, A. S. C. 'Small Data' for big insights in ecology. Trends in Ecology & Evolution, 38, 615–622 (2023). https://doi.org/10.1016/j.tree.2023.01.015

26. Guangyuan Municipal Institute of Cultural Relics Management. *Comprehensive catalogue of guangyuan grottoes: Huangze temple volume*. Wenwu Press (2008) (in Chinese).

27. Guangyuan Municipal Institute of Cultural Relics Management. *Comprehensive catalogue of guangyuan grottoes: Qianfo cliff volume* (Vols. I & II). Wenwu Press (2008) (in Chinese).

28. Abdelhakim, N. A., Salazar-Gamarra, R., Segaan, L. G., et al. Evaluation of different technologies used for extraoral surface data acquisition for 3D facial scanning. *Journal of Prosthodontics* (2025).

29. Chen, J. Ritual, canon, and image-making: Standardization in Buddhist statues of medieval China. *Artibus Asiae*, 77, 45–70 (2017).

30. Trainor, K. (ed.). Buddhism: The Illustrated Guide. Oxford University Press, 2004.

31. Harth, A., Van der Snickt, G., Schalm, O., Janssens, K., & Blanckaert, G. The young Van Dyck's fingerprint: a technical approach to assess the authenticity of a disputed painting. *Heritage Science*, 5, 22 (2017).

32. King, D. E. Dlib-ml: A machine learning toolkit. *The Journal of Machine Learning Research*, 10, 1755–1758 (2009).

33. Lundberg, S. M., & Lee, S. I. A unified approach to interpreting model predictions. In Proceedings of the 31st International Conference on Neural Information Processing Systems (pp. 4765–4774) (2017).

34. Goodfellow, I., Bengio, Y., & Courville, A. Deep learning. MIT Press (2016).

35. Yuvalı, M., Yaman, B., & Tosun, Ö. Classification comparison of machine learning algorithms using two independent cad datasets. Mathematics, 10(3), 311 (2022).

36. Sabha, M., Saffarini, M., & Yousuf, R. Image classification in cultural heritage. IAES International Journal of Artificial Intelligence (IJ-AI), 13(4), 4722–4735 (2024).

37. Ataş, M., Yeşilnacar, M. İ., & Demir Yetiş, A. Novel machine learning techniques based hybrid models (LR-KNN-ANN and SVM) in prediction of dental fluorosis in groundwater.

Environmental Geochemistry and Health, 44(11), 3891–3905 (2022).

38. Sabha, M., Saffarini, M. & Yousuf, R. Image classification in cultural heritage. *IAES International Journal of Artificial Intelligence (IJ-AI)*, 13, 4722–4735 (2024). https://doi.org/10.11591/ijai.v13.i4.pp4722-4735

39. Lumumba, V. W., Kiprotich, D., Lemasulani Mpaine, M., Grace Makena, N., & Daniel Kavita, M. Comparative analysis of cross-validation techniques: LOOCV, k-folds cross-validation, and repeated k-folds cross-validation in machine learning models (2024).

40. Zhang, H., Li, X., Zhang, B., Li, Y. & Liu, H. Spatiotemporal dynamics of Catholic church heritage in Sichuan using density weighted historical segmentation and SHAP. *npj Heritage Science*, 13, 356 (2025). https://doi.org/10.1038/s40494-025-01939-w

41. Boukrouh, I., Tayalati, F., & Azmani, A. Comparative SHAP analysis on SVM and K-NN: impacts of hyperparameter tuning on model explainability. In 2024 IEEE International Conference on Artificial Intelligence in Engineering and Technology (IICAIET) 194–198. IEEE (2024).

42. Mileva, V. R., Cowan, M. L., Cobey, K. D., et al. In the face of dominance: self-perceived and other-perceived dominance are positively associated with facial-width-to-height ratio in men. *Personality and Individual Differences*, 69, 115–118 (2014).

43. Yang, J. X. The interaction between buddhism and politics in the early Tang dynasty: a study centered on the Datang Sanzang Shengjiao Xu. *Buddhist Studies*, 01, 1–20 (2025) (in Chinese).

44. Long, H., Deng, X. H., & Wang, L. J. A preliminary study of Sui Buddhist grotto art in Bashu area. *Journal of Nanjing Arts Institute (Fine Arts & Design Edition)*, 05, 124–131+226 (2015).

45. Zhang, K. & Abdullah, M. F. W. bin. Refining the theoretical framework of modern Chinese sculpture: Insights from Buddhist imagery in the longmen grottoes. *Cogent Arts & Humanities*, 13(1), (2026). https://doi.org/10.1080/23311983.2025.2610110

46. Zhang, Z. K. The popularization of buddhism in the early tang dynasty: A study centered on the changes of imperial examination policy. Journal of Southwest Minzu University (Humanities & Social Sciences Edition), 33 (2012) (in Chinese).

47. Faure, B. The Buddhist icon and the modern gaze. *Critical Inquiry*, 24, 768–813 (1998).

48. Wu, H. From the dharma body to the corporeal body: rethinking the development of the early Tang style from a conceptual perspective. *Fudan Journal (Social Sciences Edition)*, 65(01), 126–137 (2023) (in Chinese).

49. Yang, X. Between north and south: buddhist cliff sculpture in northern sichuan in the first half of the seventh century CE. *Religions*, 15(9), 1123 (2024). https://doi.org/10.3390/rel15091123

50. Song, T. and Wang, Y., 2023. Stone Inscriptions as Mirror Images: Historical Details of Tang Dynasty Buddhism in the Luoyang Region. *Religions*, *14*(12), p.1493. https://doi.org/10.3390/rel14121493

51. Duerksen, K. N., Friedrich, T. E. & Elias, L. J. Did Buddha turn the other cheek too? A comparison of posing biases between Jesus and Buddha. *Laterality*, 21(4–6), 633–642 (2016). https://doi.org/10.1080/1357650X.2015.1087554

52. Ainsworth, M. W. Early Netherlandish painting at the crossroads: a critical look at current methodologies. In: Proceedings of a Metropolitan Museum of Art symposium on 7 November 1998. New Haven: Yale University Press (2001).

53. Zhu, J., Fang, B., Chen, T. & Yang, H. Face repairing based on transfer learning method with fewer training samples: application to a Terracotta Warrior with facial cracks and a Buddha with a broken nose. *Heritage Science*, 12(1), 186 (2024). https://doi.org/10.1186/s40494-024-01292-4

54. Hua, W., Hou, M., Qiao, Y., Zhao, X., Xu, S. & Li, S. Similarity Index Based Approach for Identifying Similar Grotto Statues to Support Virtual Restoration. *Remote Sensing*, 13(6), 1201 (2021). https://doi.org/10.3390/rs13061201

55. Ge, Y., Liu, Y., Ma, Y., Wang, Y., Guo, Y., He, J. & Mao, Y. Spatial identification and corridor network analysis of cultural heritage based on multi-model fusion: A case study of western Henan. *Ecological Indicators*, 178, 113859 (2025). https://doi.org/10.1016/j.ecolind.2025.113859

56. Buvaneshwaran, B., Ashwin, V., Abishekrupan, B. S., Sasidharan, S. & Revathi, K. P. AI Driven Restoration of Damaged Paintings and Historical Artifacts Using Generative Adversarial Networks. In *2025 3rd International Conference on Disruptive Technologies (ICDT)*, 1021–1025 (2025). https://doi.org/10.1109/icdt63985.2025.10986612

Figure Legends

Fig. 1 Comparison between Image Facial Landmark Recognition and 3D Scanning Facial Landmark Recognition.

Fig. 2 Screening criteria for selecting Buddha statues.

Fig. 3 The computational framework for chronological assessment and geometric feature engineering. a The methodological pipeline integrating high-precision 3D scanning, standardized orthographic projection, and Explainable Artificial Intelligence (XAI) to resolve chronological ambiguity. The workflow progresses from data acquisition to feature extraction, followed by multi-model machine learning classification (SVM, ANN, LR, KNN, Bayes) and SHAP-based model validation. b Extraction of 68 fiducial facial landmarks from the standardized orthographic projection, mapping the contours of the eyes, eyebrows, nose, mouth, and jawline. c Geometric feature construction based on traditional iconometric canons (Sculptural Measurement Sutra). The grid illustrates the derivation of proportional features (e.g., C, D, R) relative to the basic measurement unit S, defined as one Eye Height.

Fig. 4 Statistical divergence of facial geometric features between Phase III (Early Tang) and Phase IV (High Tang) statues. a Comparison of Local Features (A–P): Bar charts display Mean ± SD (Standard Deviation). Statistically significant differences ($P < 0.05$) are observed in the vertical expansion of Eye Height (A) and the vertical compression of the mid-face (C) and lower-face (D) in Phase IV. b Comparison of Global Features (Q, R, S, T): The dramatic reduction in the Standard Deviation of Facial Proportions (S) in Phase IV indicates a shift toward rigorous workshop standardization. The Smile Degree (Q) shows an increasing trend, correlating with the secularization of the High Tang aesthetic.

Fig. 5 Mean values of the features across statues.

Fig. 6 Explainable AI (XAI) analysis of the chronological decision boundaries. a SHAP global importance plots for Support Vector Machine (SVM), Logistic Regression (LR), and K-Nearest Neighbors (KNN). The x-axis represents the mean absolute SHAP value, quantifying the overall

magnitude of each feature's contribution. b SHAP beeswarm plots illustrating the directionality of feature impact. Each dot represents a single statue sample. Interpretation Guide: The color indicates the actual geometric measurement (Red = High Value; Blue = Low Value). The position on the x-axis indicates the impact on the model's decision: dots shifted to the right (positive SHAP value) increase the probability of classifying the statue into the target phase. Example: In the Phase III panel (left column), the feature Eye-to-Nose Distance (C) shows red dots clustered on the right side. This indicates that high values of Feature C (a longer mid-face) increase the probability of Phase III classification, mathematically confirming the "long mid-face" aesthetic of the Early Tang. Conversely, Eye Height (A) shows blue dots on the right, meaning low values (narrower eyes) are predictive of Phase III.